Biochemical Journal (2018) **475** 2861–2875
https://doi.org/10.1042/BCJ20180457

Research Article

Thermodynamic and functional characterization of the periplasmic triheme cytochrome PpcA from *Geobacter metallireducens*

Tomás M. Fernandes, Leonor Morgado and Carlos A. Salgueiro

UCIBIO-Requimte, Departamento de Química, Faculdade de Ciências e Tecnologia, Universidade NOVA de Lisboa, Campus Caparica, 2829-516 Caparica, Portugal

Correspondence: Carlos A. Salgueiro (csalgueiro@fct.unl.pt)

The *Geobacter metallireducens* bacterium can couple the oxidation of a wide range of compounds to the reduction of several extracellular electron acceptors, including pollutants or electrode surfaces for current production in microbial fuel cells. For these reasons, *G. metallireducens* are of interest for practical biotechnological applications. The use of such electron acceptors relies on a mechanism that permits electrons to be transferred to the cell exterior. The cytochrome PpcA from *G. metallireducens* is a member of a family composed of five periplasmic triheme cytochromes, which are important to bridge the electron transfer from the cytoplasmic donors to the extracellular acceptors. Using NMR and visible spectroscopic techniques, a detailed thermodynamic characterization of PpcA was obtained, including the determination of the heme reduction potentials and their redox and redox-Bohr interactions. These parameters revealed unique features for PpcA from *G. metallireducens* compared with other triheme cytochromes from different microorganisms, namely the less negative heme reduction potentials and concomitant functional working potential ranges. It was also shown that the order of oxidation of the hemes is pH-independent, but the protein is designed to couple e^-/H^+ transfer exclusively at physiological pH.

Introduction

Geobacter species are abundant Gram-negative bacteria playing an important biogeochemical role in a diversity of natural environments. These bacteria are mostly known for their capability of making electrical contacts with extracellular electron acceptors and other microorganisms. They show an impressive respiratory versatility, being capable of sustaining their growth by using extracellular compounds as terminal electron acceptors, such as Fe(III), U(VI) or Mn(IV) oxides, in addition to the more frequent respiratory processes, that utilize both soluble electrons donors (e.g. acetate) and acceptors (e.g. fumarate) [1]. Some electron acceptors that can be used by *Geobacter* cells are toxic or radioactive [2–7]. In addition, *Geobacter* species produce higher current densities than any other known microorganism in microbial fuel cells [8]. Such features make *Geobacter* bacteria preferential targets for bioremediation and bioenergy applications [9,10].

Geobacter sulfurreducens was the first *Geobacter* family member for which genetic manipulation methods were developed [11]. Consequently, it has been used as the first choice for genomic and proteomic studies aiming to elucidate the bacteria's metabolism, gene regulation and extracellular electron transfer mechanisms [11–18]. On the other hand, *Geobacter metallireducens* was the first identified member of the *Geobacter* species [1,19,20] and the first microorganism found to completely oxidize organic compounds to carbon dioxide, with Fe(III) oxide serving as the electron acceptor [3,20,21]. This bacterium was firstly isolated from freshwater sediments and shares several metabolic features with *G. sulfurreducens*. Furthermore, *G. metallireducens* is also able to oxidize short-chain fatty acids, alcohols and monoaromatic compounds, such as toluene and phenol [19,22]. It is also

Received: 14 June 2018
Revised: 30 July 2018
Accepted: 1 August 2018

Accepted Manuscript online: 2 August 2018
Version of Record published: 14 September 2018

Biochemical Journal (2018) **475** 2861–2875
https://doi.org/10.1042/BCJ20180457

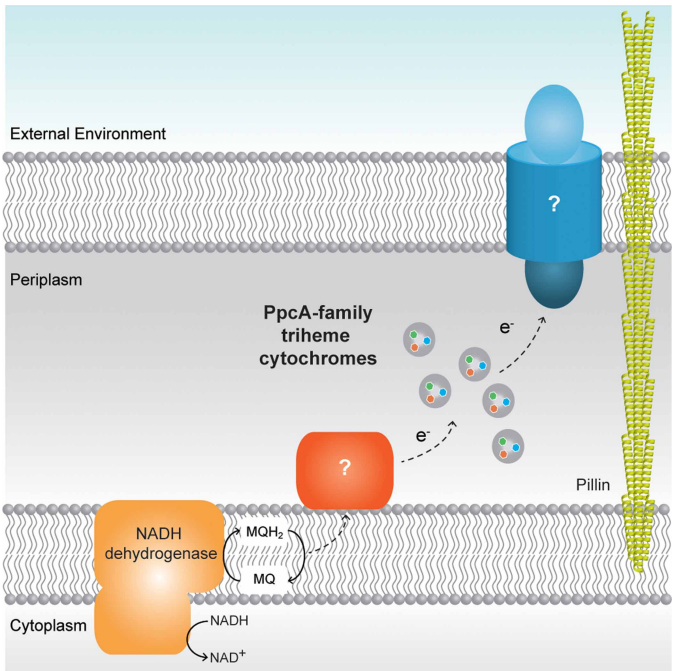

Figure 1. Extracellular electron transfer in *Geobacter metallireducens*.
The periplasmic PpcA-family triheme cytochromes mediate the electron transfer between the inner membrane-associated cytochromes (in red) and the porin–cytochrome complexes in the outer membrane (in blue).

capable of storing energy through dissimilatory reduction of iron, manganese, uranium and other metals [21,23,24], as well as nitrate [19,25,26]. The broad range of compounds that can be metabolized by *G. metallireducens* compared with *G. sulfurreducens* opens promising routes for biotechnological applications [20–23].

The recent development of a genetic system for *G. metallireducens* [27] has refocused attention on this bacterium. Compared with *G. sulfurreducens*, for which several proteomic and genetic studies have identified key electron transfer components for the extracellular electron transfer mechanisms [12,14,15,28–35], very few are available for *G. metallireducens* [36,37]. The genome of *G. metallireducens* was sequenced and it encodes for 91 *c*-type cytochromes, of which 65 have homologs in *G. sulfurreducens* [23,38]. These include proteins located on the inner membrane, periplasm and on the outer membrane. In the periplasm, the so-called PpcA family composed by triheme periplasmic cytochromes has been shown to have a crucial role in the regulation of the electron flow towards extracellular electron acceptors (Figure 1). For this reason, the PpcA-family cytochromes can potentially be explored to develop rational *Geobacter*-mutated strains with increased respiratory rates and optimal current production in microbial fuel cells.

A preliminary biochemical characterization of the cytochrome PpcA from *G. metallireducens* suggested that the protein could exhibit different functional properties compared with its homologs in *G. sulfurreducens* [39]. Therefore, in the present work, we performed a detailed thermodynamic characterization of the cytochrome PpcA from *G. metallireducens* using NMR and visible spectroscopic techniques. The study showed that the heme reduction potential values differ considerably from the ones observed for homolog proteins in different microorganisms and are modulated by redox and redox-Bohr interactions, conferring unique functional features to the protein.

Materials and methods

Expression and purification of triheme cytochrome PpcA from *G. metallireducens*

PpcA from *G. metallireducens* was produced and purified as recently described [39]. Briefly, *Escherichia coli* BL21 (DE3) cells, containing the plasmid pEC86 (encoding for the cytochrome *c* maturation gene cluster

ccmABCDEFGH and a chloramphenicol-resistance gene), were co-transformed with the plasmid pCSGmet2902 (containing the gene *Gmet_2902*, encoding for *G. metallireducens* PpcA and carrying an ampicillin-resistance gene). Cells were then grown at 30°C in 2×YT media, supplemented with 34 μg/mL chloramphenicol and 100 μg/mL ampicillin, to an OD_{600} of ∼1.5. Protein expression was then induced with 10 μM of isopropyl β-D-thiogalactoside (IPTG) and the cell cultures grown overnight at 30°C. Following overnight incubation, cells were harvested by centrifugation at 4000×***g*** for 20 min. The periplasmic fraction was obtained after cells were incubated in lysis buffer [100 mM Tris–HCl (pH 8.0), 0.5 mM EDTA, 20% sucrose and 0.5 mg/mL lysozyme] for 15 min. This fraction was recovered by centrifugation at 14 700×***g***, at 4°C for 20 min. The supernatant was further ultracentrifugated at 225 000×***g***, at 4°C for 1 h. The final supernatant obtained was dialyzed against 2 × 4.5 L of 10 mM Tris–HCl (pH 8.0) and loaded onto 2 × 5 mL Bio-Scale™ Mini UNOsphere™ S cartridges (Bio-Rad), equilibrated with the same buffer. The protein was eluted with a sodium chloride gradient (0–300 mM), and the obtained fraction was concentrated to 1 mL before injection in a Superdex 75 molecular exclusion column (GE Healthcare), equilibrated with 100 mM sodium phosphate buffer (pH 8.0). Protein purity was evaluated by Coomassie-stained SDS–PAGE. The concentration of the cytochrome was determined by measuring the absorbance of the reduced form at 552 nm, using the extinction coefficient of 118 mM^{-1} cm^{-1} [39].

NMR spectroscopy

Sample preparation

Samples for NMR studies at intermediate levels of oxidation were prepared with ∼80 μM concentration, in 80 mM phosphate buffer prepared in pure ^2H_2O (CIL isotopes), at different pH values, with NaCl (250 mM of final ionic strength). The protein samples used to assign the heme methyl chemical shifts both in the fully reduced and fully oxidized states were prepared with ∼750 μM concentration in the same buffer at pH 5.8 and 8.1. The pH values of the samples were verified with a glass microelectrode. For sample reduction, the NMR tubes were sealed with a gas-tight serum cap and the air was flushed out from the sample, to avoid possible oxidation of the samples. Then, the samples were reduced directly in the NMR tube with gaseous hydrogen in the presence of catalytic amounts of hydrogenase from *Desulfovibrio vulgaris* (Hildenborough). The partially oxidized samples, used for the NMR redox titrations, were obtained by first removing the hydrogen from the reduced sample with nitrogen and then adding controlled amounts of air into the NMR tube with a Hamilton syringe.

NMR experiments

All the NMR experiments were acquired in a Bruker Avance III 600 MHz spectrometer equipped with a triple-resonance cryoprobe (TCI) at 15°C. The ^1H chemical shifts were calibrated using the water signal as an internal reference. All the different spectra obtained were processed using TopSpin3.5.7™ (Bruker BioSpin, Karlsruhe, Germany).

Redox titrations

The oxidation patterns of PpcA from *G. metallireducens* were monitored by 2D ^1H-EXchange SpectroscopY (EXSY), at different pH values. All the 2D EXSY spectra were accumulated with a mixing time of 25 ms, collecting 2048 (t_2) × 256 (t_1) data points to cover a sweep width of 27.5 kHz, with 256 scans per increment. 1D ^1H-NMR spectra were obtained before and after each 2D NMR spectrum to check for any changes in the oxidation state of the sample during the 2D NMR experiment. The 1D NMR spectra were acquired with water pre-saturation collecting 32k data points to cover a spectral width of 33 kHz.

Fully reduced state experiments

For the assignment of the heme methyl substituents in the fully reduced state, 2D ^1H-NOESY and 2D ^1H-TOCSY experiments were acquired using pulse sequences with water pre-saturation. The 2D ^1H-NOESY spectra were acquired with a mixing time of 80 ms, collecting 2048 (t_2) × 256 (t_1) data points to cover a sweep width of 8.4 kHz, with 160 scans per increment. The 2D ^1H-TOCSY spectra were acquired with a mixing time of 60 ms, 128 scans and with the same number of data points and spectral width.

Biochemical Journal (2018) **475** 2861–2875
https://doi.org/10.1042/BCJ20180457

Fully oxidized state experiments

For the assignment of the heme methyl substituents of the protein in the fully oxidized state, the following set of 2D NMR experiments was acquired: 2D ^{1}H,^{13}C-HMQC, 2D ^{1}H-NOESY and 2D ^{1}H-TOCSY. The 2D ^{1}H,^{13}C-HMQC spectra were acquired collecting 4096 (t_2) × 256 (t_1) data points to cover a sweep width of 28.8 kHz in the ^{1}H dimension and 52.8 kHz in the ^{13}C dimension, with 360 scans per increment. The 2D ^{1}H-NOESY spectra were acquired with a mixing time of 80 ms, collecting 4096 (t_2) × 512 (t_1) data points to cover a sweep width of 28.8 kHz, with 200 scans per increment. The 2D ^{1}H-TOCSY spectra were acquired with a mixing time of 45 ms, collecting 2048 (t_2) × 512 (t_1) data points to cover a sweep width of 28.8 kHz, with 160 scans per increment.

Thermodynamic model

The cytochrome PpcA from *G. metallireducens* contains three low-spin bis-histidinyl axial coordination heme groups with identical optical properties [39]. Consequently, it is not possible to discriminate the individual heme oxidation patterns using visible spectroscopy. In addition, the coexistence of several microstates in solution makes the study of multiheme cytochromes, containing identical redox centers, particularly challenging. In fact, in the specific case of a triheme cytochrome, three consecutive reversible steps of one-electron transfer convert the fully reduced into the fully oxidized state. Therefore, four different redox stages, numbered S_0 to S_3, can be defined. At each stage, microstates are grouped with the same number of oxidized hemes (Figure 2).

As a consequence of the close spatial disposition of the heme groups in small multiheme cytochromes, as it is the case of PpcA from *G. metallireducens* [39], the redox potential of one heme is modulated by the oxidation state of its neighbors (redox interactions, g_{ij}, Figure 2A). Moreover, the redox potential of the hemes can also be modulated by the pH (redox-Bohr effect). The magnitude of this effect is determined by the so-called redox-Bohr interactions (g_{iH}, Figure 2A), which measure the effect of the protonation state of the redox-Bohr center (a protonable center, located in the vicinity of the hemes) on the heme redox potentials. The 16 microstates that can coexist in solution for a triheme cytochrome containing one redox-Bohr center are illustrated in Figure 2B. The fractional contribution of the 16 microstates, across the full range of pH and solution potential, can be defined by 10 thermodynamic parameters: the three heme oxidation energies (reduction potentials), the pK_a of the redox-Bohr center, the three interaction energies between each pair of hemes (redox interactions) and the three interaction energies between each heme and the redox-Bohr center (redox-Bohr interactions) (for a review, see [40,41]). The energy of each microstate relative to the reference microstate (fully reduced and protonated, P_{0H}) is then given by a simple sum of the appropriate energy terms among the four independent centers, the six possible two-center interactions and one term that accounts for the effect of the solution potential (SFE) in the oxidation stage S (eqn 1), and another for the proton chemical potential (2.3RTpH) added for the deprotonated forms (eqn 2):

$$G_{iH} = \Sigma g_i + \Sigma g_{ij} - \mathrm{SFE} \tag{1}$$

$$G_i = G_{iH} + g_H + \Sigma g_{iH} - 2.3\ \mathrm{RTpH} \tag{2}$$

where *iH* designates a particular protonated microstate with oxidized heme(s) group(s) i (i = 1–3); g_i the energy of oxidation of heme i; g_{ij} the interaction energy between each pair of hemes i and j; g_H the deprotonation energy of the fully reduced protein; g_{iH} the energy of interaction between the hemes and the redox-Bohr center; S the oxidation stage (that corresponds to the number of oxidized hemes) and E the redox potential of the solution.

The energy values can be converted to reduction potentials using the following equation:

$$\Delta G = -nF\Delta E \tag{3}$$

and the fractional contribution of each microstate (P_i) can be determined by the Boltzmann equation (eqn 4):

$$P_i = \exp^{-G_i/(\mathrm{RT})} \tag{4}$$

Biochemical Journal (2018) **475** 2861–2875
https://doi.org/10.1042/BCJ20180457

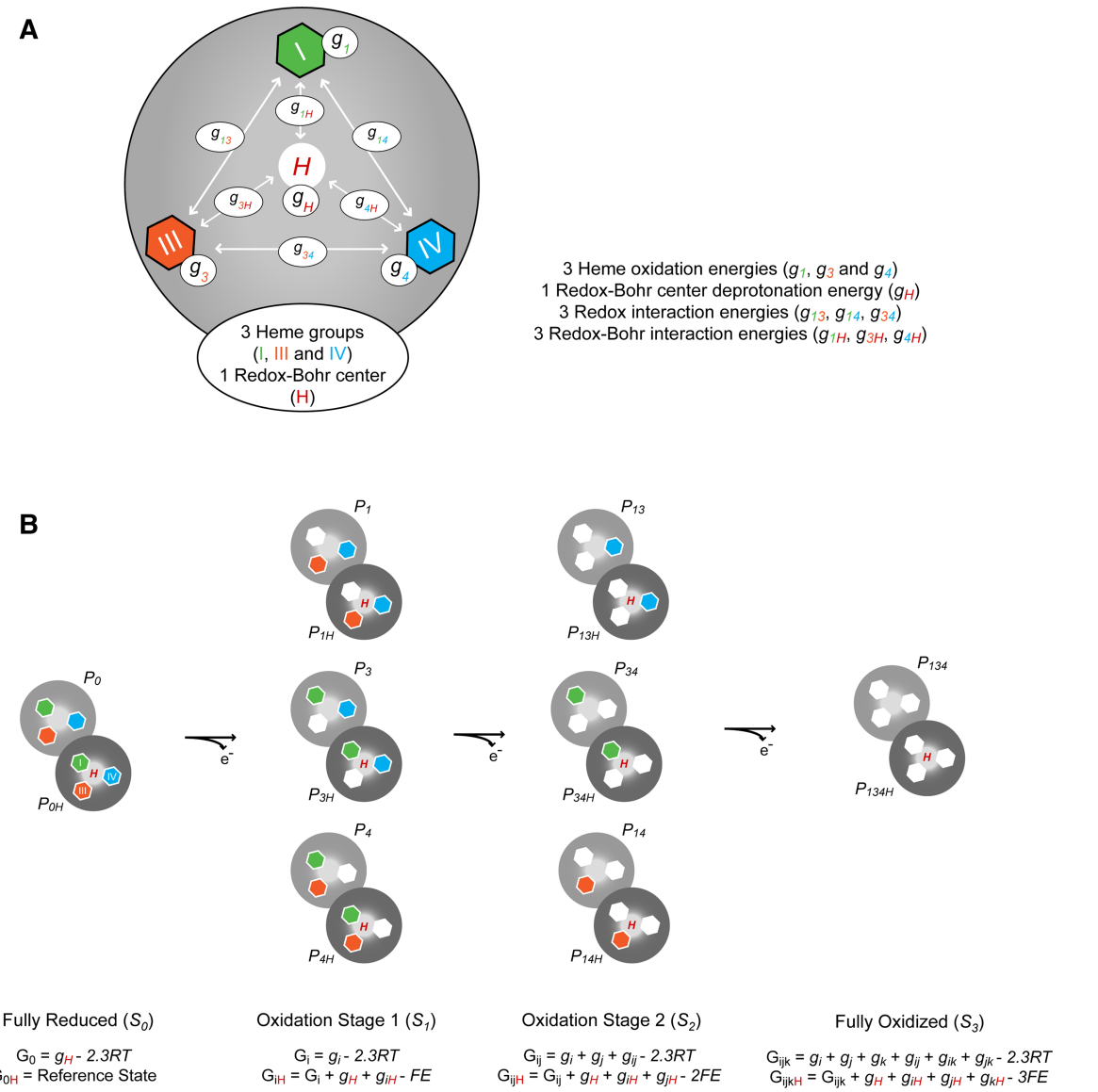

Figure 2. Thermodynamic model for a triheme cytochrome with one redox-Bohr center.

(**A**) Schematic representation of the interaction networks of a multiheme cytochrome with three hemes [inner hexagons, numbered I (green), III (orange) and IV (blue)] and one redox-Bohr center (red 'H'). The terms g_{ij} and g_{iH} represent the interaction energies between the hemes (*ij*) and between the hemes and the redox-Bohr center (*H*), respectively. The individual heme oxidation energies are represented as g_1, g_3 and g_4 for hemes I, III and IV, respectively. The 10 energy parameters that describe the full interaction networks are listed next to the figure. (**B**) Electronic distribution scheme for a triheme cytochrome with a proton-linked equilibrium, showing the 16 possible microstates. The light gray and dark gray circles correspond to the deprotonated and protonated microstates, respectively. The protonated microstates are also identified with a red 'H', which mimics the redox-Bohr center. The reduced hemes I, III and IV are colored green, orange and blue, respectively. The oxidized hemes are colored white. The microstates are grouped, according to the number of oxidized hemes, in four oxidation stages connected by three one-electron redox steps. P_{0H} and P_0 represent the reduced protonated and deprotonated microstates, respectively. P_{ijkH} and P_{ijk} indicate, respectively, the protonated and deprotonated microstates, where *i*, *j* and *k* represent the heme(s) that are oxidized in that particular microstate. G_{0H} and G_0 represent the energies of the reduced protonated and deprotonated microstates, respectively. G_{ijkH} and G_{ijk} represent the energies of the protonated and deprotonated microstates, respectively. For details see eqns (1) and (2) in the thermodynamic model section.

Biochemical Journal (2018) **475** 2861–2875
https://doi.org/10.1042/BCJ20180457

In experimental terms, the thermodynamic parameters can be determined by combining data obtained from NMR and visible redox titrations when the intramolecular electron exchange rate (between microstates within the same oxidation stage) is fast and the intermolecular electron exchange rate (between microstates belonging to different oxidation stages) is slow on the NMR time scale (for a review, see [40,41]). In this case, the heme proton signals have different chemical shifts in each oxidation stage and can be discriminated by 2D ^{1}H-EXSY NMR experiments. Therefore, by following the chemical shifts of one heme methyl group (m) for each heme from their position in the reduced state to their final position in the oxidized state, it is possible to monitor the stepwise oxidation of the hemes. At each pH, a methyl group of any heme, i, in the oxidation stage S has a single peak at a position $\delta^{m,S}_{obs}$. This shift depends on the populations of the microstates in which that heme is oxidized (since there is fast intramolecular electron exchange within each stage) weight-averaged according to the deprotonated and protonated populations (eqn 5):

$$\delta^{m,S} = \frac{(\delta^{m,3} - \delta^{m,0})\sum P_{m,S} + (\delta_H{}^{m,3} - \delta^{m,0})\sum P^{H}_{m,S}}{\sum P_S} + \delta^{m,0} \quad (5)$$

where $\delta^{m,0}$ is the observed chemical shift of methyl m in the fully reduced protein (stage S_0), and $\delta^{m,3}$ and $\delta^{m,3}_H$ are those observed in the fully oxidized (stage S_3) deprotonated or protonated protein, respectively; $\sum P_{m,S}$ and $\sum P^{H}_{m,S}$ are the sums over all the populations with heme m oxidized in stage S, deprotonated or protonated, respectively; and $\sum P_S$ is the sum over all the populations, protonated and deprotonated in stage S (Figure 2).

However, the information collected by the 2D ^{1}H-EXSY NMR redox titrations at different pH values only defines the relative values for the heme reduction potentials and interactions. The absolute values are obtained from the simultaneous fitting of the NMR data (eqn 5) and protein-reduced fractions (F_{red}, eqn 6), obtained from redox titrations followed by visible spectroscopy at two different pH values, using the Marquardt method [40].

$$F_{red} = \frac{3\sum P_{S,0} + 2\sum P_{S,1} + \sum P_{S,2}}{3\sum P_S}. \quad (6)$$

In this equation, $\sum P_{S,0}$, $\sum P_{S,1}$ and $\sum P_{S,2}$ are the sums over all the populations in stages 0, 1 and 2, respectively.

In the present work, the stepwise oxidation of the hemes in the cytochrome PpcA from *G. metallireducens* was measured by 2D ^{1}H-EXSY NMR experiments, acquired in the pH range of 5.8–8.9. These data were then fitted simultaneously with the visible redox titrations previously obtained at pH 7 and 8 [39]. The experimental uncertainty of the NMR data was evaluated from the linewidth of each NMR signal at half height, whereas the visible data points were estimated to have an uncertainty of 3% of the total optical signal.

Results and discussion

Probing the order of oxidation of the heme groups

The heme groups of the cytochrome PpcA are low-spin in the reduced (Fe(II), $S = 0$) and oxidized (Fe(III), $S = 1/2$) states. Consequently, this cytochrome displays considerably different, but well-resolved NMR spectra in both states [39]. Of all the heme substituents, the methyl groups are the most appropriate to probe the heme oxidation profiles. On one hand, the three-proton intensity of these signals facilitates their assignment and on the other hand, their signals shift from crowded regions in the reduced NMR spectrum to relatively empty spectral regions in the oxidized state (see Figure 3A). In the reduced state, the protein is diamagnetic, and thus, the heme proton chemical shifts are essentially dominated by the heme ring-current effects and are found in well-defined regions of the spectra (typically between 2.5 and 4.5 ppm). On the contrary, due to the presence of one unpaired electron per heme in the oxidized state, the heme methyl signals are considerably spread all over the entire spectral width, which further complicates their assignment. The assignment of the heme methyls signals in the reduced form was previously obtained at pH 7.1 and 25°C [39] and was redone in the present work at the experimental conditions used to monitor the heme oxidation profiles (Supplementary Table S1).

As described above, the individual heme oxidation profiles can be monitored by 2D ^{1}H-EXSY NMR experiments if the intra- and intermolecular electron exchange rates are fast and slow on the NMR time scale, respectively. The 2D ^{1}H-EXSY NMR spectra obtained for the samples at intermediate levels of oxidation show

Biochemical Journal (2018) **475** 2861–2875
https://doi.org/10.1042/BCJ20180457

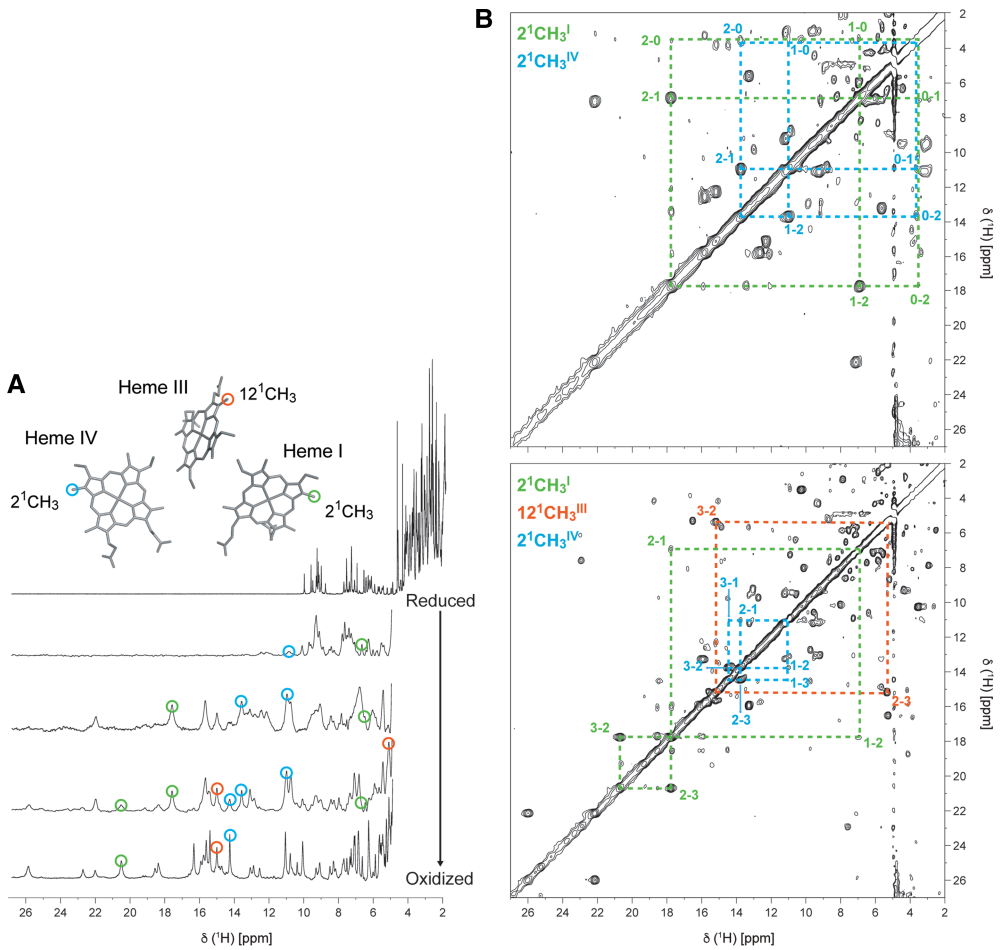

Figure 3. Illustration of the heme oxidation profiles for PpcA from *G. metallireducens* (pH 5.8, 15°C).
(**A**) The 1D ^{1}H-NMR spectra, acquired at different stages of oxidation, illustrate the redox titration of the cytochrome. The peaks corresponding to the heme methyls 2^{1}CH$_3^I$, 12^{1}CH$_3^{III}$ and 2^{1}CH$_3^{IV}$ (labeled accordingly to the IUPAC nomenclature for tetrapyrroles [52]) are marked by green, orange and blue circles, respectively. These heme methyls are also highlighted with the same color code in the heme core of PpcA from *G. sulfurreducens* (PBD code: 2MZ9 [53]). (**B**) In the expansions of the 2D ^{1}H-EXSY NMR spectra, the cross-peaks resulting from intermolecular electron transfer between the different oxidation stages (0–3) are indicated by dashed lines for heme methyls 2^{1}CH$_3^I$ (green), 12^{1}CH$_3^{III}$ (orange) and 2^{1}CH$_3^{IV}$ (blue). The hemes are numbered I, III and IV, a designation that derives from the superimposition with those of the structurally homologous tetraheme cytochromes c_3 [54].

that the cytochrome PpcA from *G. metallireducens* meets these requirements in the experimental conditions used, since the heme methyl signals can be followed throughout the different oxidation stages (Figure 3B).

The chemical shifts of the heme methyls in the reduced state constitute excellent starting points to monitor their variation up to their final position in the fully oxidized state. However, when the hemes show a very small percentage of oxidation in the first oxidation steps, the variation in their chemical shifts is also very small so that the exchange connectivities are placed at or near the diagonal of the spectra. This is exactly the case for one of the heme groups in PpcA, as illustrated by the 2D ^{1}H-EXSY NMR spectrum obtained at early stages of oxidation in Figure 3B. In fact, only connectivities between oxidation stages 0 and 1 for hemes I and IV could be observed. As discussed below, the first oxidation step is essentially dominated by the oxidation of heme IV, followed by heme I, which prevents the observation of connectivities between oxidation stages 0 and 1 for heme III. As a consequence, it was not possible to monitor the stepwise oxidation of heme III starting from the fully reduced state. To overcome this, the assignment of the heme methyls was also carried out in the fully oxidized state, by the combined analysis of 2D ^{1}H-NOESY, 2D ^{1}H-TOCSY and 2D ^{1}H,^{13}C-HMQC NMR spectra,

Biochemical Journal (2018) **475** 2861–2875
https://doi.org/10.1042/BCJ20180457

Table 1 Redox-dependence of the heme methyl proton chemical shifts and heme oxidation fractions of PpcA from *G. metallireducens* (pH 5.8 and 15°C).

The heme methyls $2^1CH^{I}_3$, $12^1CH^{III}_3$ and $2^1CH^{IV}_3$ were chosen to monitor each heme oxidation through the four oxidation stages (see text). The heme oxidation fractions, x_i, in each stage of oxidation were calculated according to the equation $x_i = (\delta_i - \delta_0)/(\delta_3 - \delta_0)$, where δ_i, δ_0 and δ_3 are the observed chemical shifts of the heme methyl in stage *i*, *0* (fully reduced) and *3* (fully oxidized), respectively. The heme methyl signal not detected is indicated by 'n.d.'.

	Chemical shift (ppm)			x_i			
Oxidation stage	**I**	**III**	**IV**	**I**	**III**	**IV**	**Σ x_i**
0	3.55	3.51	3.65	0	0	0	0
1	6.93	n.d.[1]	11.03	0.20	0.12[1]	0.68	1.00
2	17.78	5.33	13.76	0.83	0.16	0.94	1.93
3	20.71	15.18	14.43	1	1	1	3

[1]The chemical shift of methyl $12^1CH^{III}_3$ in the oxidation stage 1 is located underneath the water signal and is not observable. Thus, the oxidation fraction of heme III was estimated from the values obtained for the other hemes.

following a strategy previously described [42–44] (Supplementary Table S1). The chemical shifts of the heme methyls in the oxidized state were then used to follow signals backward to their position at intermediate oxidation states. This strategy allowed us to monitor the stepwise oxidation of each heme in the pH range of 5.8–8.9. As an example, the heme oxidation profiles of the cytochrome, at pH 5.8, are illustrated by the heme methyls $2^1CH^{I}_3$, $12^1CH^{III}_3$ and $2^1CH^{IV}_3$ in Figure 3B. The correspondent oxidation fraction values are listed in Table 1. In the typical arrangement of the heme core of a triheme cytochrome, the selected methyl groups for each heme point away from neighboring hemes (see Figure 3A) and, consequently, the extrinsic contribution to their chemical shifts from the oxidation of neighboring hemes is minimized. The analysis of Table 1 confirms that the extrinsic shifts for the selected heme methyls are not significant, since the sums of the oxidation fractions at each oxidation stage are close to integers and, therefore, each methyl reflects the oxidation state of its own heme. The heme oxidation fractions obtained at pH 5.8 show that heme IV clearly dominates the first oxidation step (68%). The largest fractional oxidation of heme I is obtained in the second step (63%), followed by heme III in the last step (84%).

Thermodynamic properties

To determine the thermodynamic parameters of PpcA, the pH dependence of the heme methyl chemical shifts, in the pH range of 5.8–8.9, together with the data from visible redox titrations obtained at pH 7 and 8 [39], was fitted to the model summarized in the Materials and Methods section (Figure 4). The quality of the fittings obtained clearly shows that the thermodynamic properties of PpcA are well described by the model that considers three heme groups and one redox-Bohr center (Figure 2). The thermodynamic parameters and the macroscopic pK_a values associated with the four stages of oxidation are indicated in Table 2. The parameters show that the microscopic reduction potentials of the hemes are different and negative: −80, −70 and −113 mV for hemes I, III and IV, respectively. Compared with the data available for homologous cytochromes, the reduction potentials of the hemes in PpcA from *G. metallireducens* are considerable less negative, though at a smaller extent for heme IV (cf. Tables 2 and 3). The structural analysis carried out by the comparison of the heme substituents and backbone NMR chemical shifts of PpcA from *G. metallireducens*, with those obtained for the homologous cytochrome from *G. sulfurreducens* showed that the non-conserved residues are responsible for important local conformational changes in the vicinity of hemes I and III [39], which might explain the differences observed in the reduction potential values.

The thermodynamic parameters of PpcA from *G. metallireducens* also showed that the redox interactions for each pair of hemes are positive, indicating that the oxidation of one heme makes difficult the oxidation of its neighbor. As expected from the heme core architecture (see Figure 3A), the higher redox interaction values are of the same magnitude and are observed for the closest pairs of hemes: I–III (35 mV) and III–IV (37 mV). Furthermore, the redox-Bohr interactions are negative, which indicates that the removal of proton(s), upon deprotonation of the redox-Bohr center, lowers the affinity for electrons by the heme groups (lower reduction

Biochemical Journal (2018) **475** 2861–2875
https://doi.org/10.1042/BCJ20180457

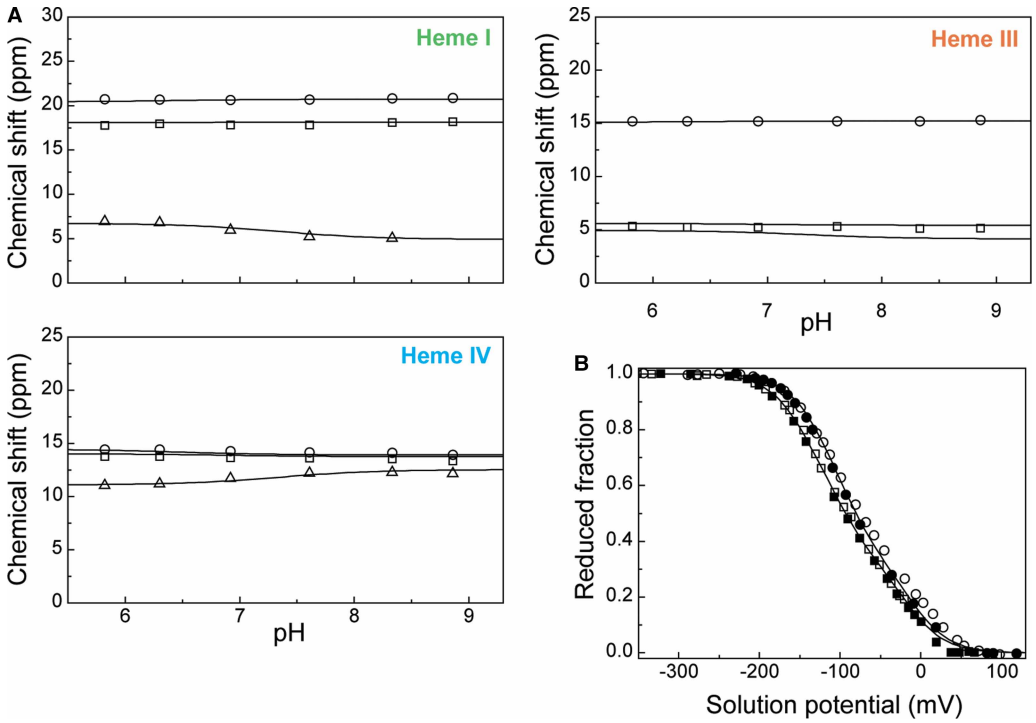

Figure 4. Fitting of the thermodynamic model to the experimental data for PpcA from *G. metallireducens*.
The solid lines are the result of the simultaneous fitting of the NMR (**A**) and visible data (**B**). In the panel (**A**), the figures show the pH dependence of heme methyl chemical shifts at oxidation stages *1* (Δ), *2* (□) and *3* (○). The chemical shift dependence of the heme methyls in the fully reduced stage (stage *0*) is not plotted since they are unaffected by the pH. In the panel (**B**), the figure corresponds to the reduced fractions of the cytochrome, determined by visible spectroscopy at pH 7 (○) and pH 8 (□). In both panels, the open and filled symbols represent the data points in the reductive and oxidative titrations, respectively.

potential values) and *vice versa*. Heme IV shows the higher redox-Bohr interaction (−49 mV), which suggests that the redox-Bohr center is located in its vicinity. This was independently confirmed by the analysis of the pH dependence of all heme methyl chemical shifts in the oxidized state, which showed that methyl $12^{1}CH_{3}^{IV}$ is clearly the most affected one (Figure 5).

Table 2 Thermodynamic parameters for PpcA from *G. metallireducens* in the fully reduced and protonated form.

	Energy (meV)			
	Heme I	**Heme III**	**Heme IV**	**Redox-Bohr center**
Heme I	**−80 (6)**	35 (4)	3 (5)	−22 (6)
Heme III		**−70 (7)**	37 (7)	−23 (7)
Heme IV			**−113 (6)**	−49 (6)
Redox-Bohr center				**463 (13)**

Diagonal values (in bold) correspond to the oxidation energies of the hemes and deprotonating energy of the redox-Bohr center. Off-diagonal values are the redox (heme–heme) and redox-Bohr (heme–proton) interaction energies. All energies are reported in meV, with standard errors given in parenthesis.
The macroscopic pK_a values of the redox-Bohr center in each stage of oxidation, calculated from the redox-Bohr center parameters, are the following: 8.1 (stage 0); 7.3 (stage 1); 6.9 (stage 2) and 6.5 (stage 3).
The pK_a of the reduced and oxidized protein is given by $g_H F/(2.3RT)$ and $\left(g_H + \sum_{i=1}^{3} g_{iH}\right) F/(2.3RT)$, respectively.

Biochemical Journal (2018) **475** 2861–2875
https://doi.org/10.1042/BCJ20180457

Table 3 Heme reduction potentials of triheme cytochromes from *G. metallireducens* (*Gm*), *G. sulfurreducens* (*Gs*) and *Desulfuromonas acetoxidans* (*Da*) in the fully reduced and protonated state.

The values are relative to the NHE.

	Heme reduction potentials (mV)		
Cytochrome	**Heme I**	**Heme III**	**Heme IV**
Gm PpcA (present work)	−80	−70	−113
Gs PpcA [50]	−154	−138	−125
Gs PpcB [50]	−150	−166	−125
Gs PpcD [50]	−156	−139	−149
Gs PpcE [50]	−167	−175	−116
Da c_7 [51]	−201	−200	−142

Effect of the pH on the heme oxidation profiles

We have shown recently that the visible redox titration curves are pH-dependent (redox-Bohr effect) [39]. The data obtained in the present work clearly confirms this observation, as the macroscopic pK_a values of the redox-Bohr center are significantly different in the reduced and oxidized states (8.1 and 6.5, respectively — see Table 2). From the thermodynamic parameters (Table 2), it is possible to establish the order of oxidation of the hemes for the fully reduced and protonated protein, which is IV–I–III (−113, −80 and −70 mV, respectively). As mentioned before, the negative redox-Bohr interactions decrease the affinity of the hemes for electrons. This is, in fact, reflected in the heme reduction potentials of the fully reduced and deprotonated protein, which can be obtained by the simple sum of the heme reduction potentials of the fully reduced and protonated state with their respective redox-Bohr interactions: −162, −102 and −93 mV for hemes IV, I and III, respectively (see Table 2).

Since the solution pH modulates the affinity of the hemes for electrons in PpcA, we further analyzed the individual heme oxidation profiles inside and outside the physiological pH range (Figure 6). The shape of the heme redox curves differs from a pure Nernst curve, which indicates that the heme electron affinity is also modulated by the heme–heme redox interactions. This is particularly notorious for heme III at pH 5 (see

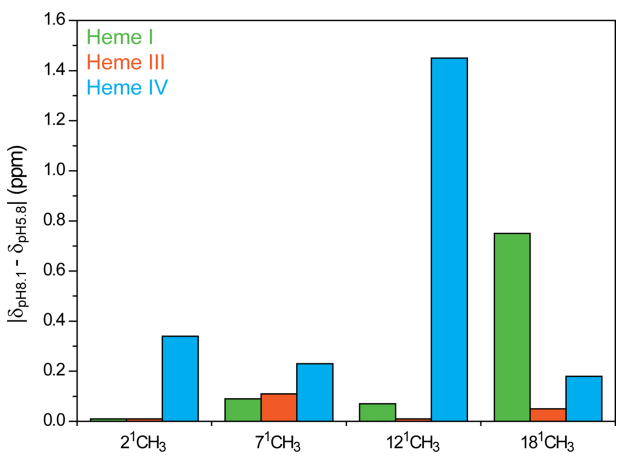

Figure 5. pH dependence of the heme methyl proton chemical shifts of PpcA from *G. metallireducens* in the oxidized state.

The chemical shift variations were calculated between pH 8.1 and 5.8. The green, orange and blue bars represent the variations observed for the hemes I, III and IV methyl substituents, respectively. Complete lists of the assigned heme methyls are provided in Supplementary Tables S1 and S2.

Biochemical Journal (2018) **475** 2861–2875
https://doi.org/10.1042/BCJ20180457

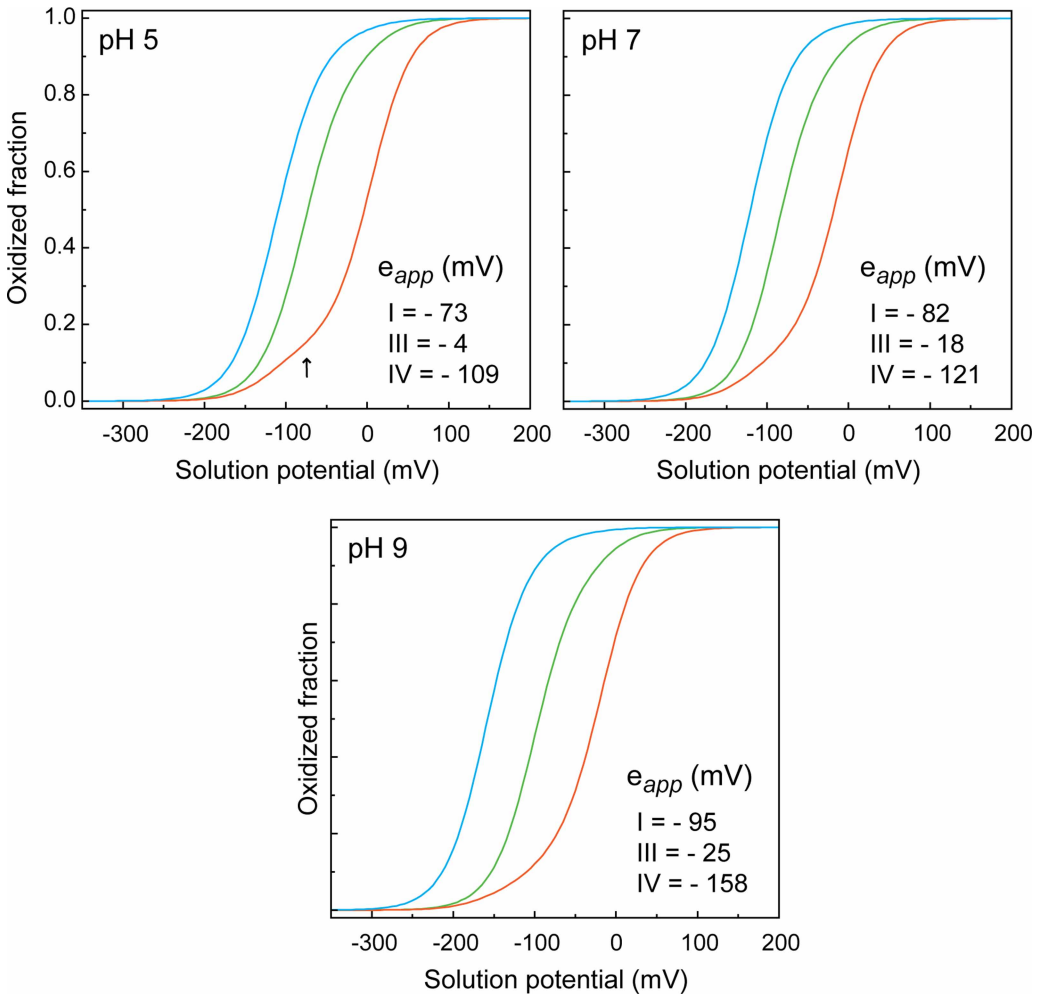

Figure 6. Redox-dependence of the heme oxidation fractions of PpcA from *G. metallireducens* at different pH values.
The curves were calculated as a function of the solution reduction potential (relative to NHE) using the parameters listed in Table 2. The midpoint reduction potentials of the hemes (e_{app}) are also indicated.

arrow in Figure 6). In fact, at low pH, the e_{app} values (i.e. the point at which the oxidized and reduced fractions of each heme group are equally populated) of the first two hemes to oxidize (hemes I and IV) are close to each other. Consequently, as their oxidation progresses, the oxidation curve of heme III shifts to higher reduction potential values as a result of the large redox interactions with hemes I and IV (35 and 37 mV, respectively).

Overall, the individual heme oxidation profiles in the pH range of 5–9 show that the relative order of oxidation remains unaltered (Figure 6). This is explained by the largest redox-Bohr interaction showed by heme IV (−49 mV), the first heme to oxidize, compared with the nearly identical redox-Bohr interactions of hemes I and III (−22 and −23 mV, respectively). Although the order of oxidation of the heme groups is independent of the pH, the redox-Bohr center still plays a role in the modulation of the e_{app} values, as they decrease with the solution pH (Figure 6). Owing to the higher redox-Bohr interaction, this is particularly notorious for the heme IV curve, which progressively deviates from those of the other hemes with the increase in pH (Figure 6).

Functional mechanism at physiological pH

The redox-Bohr effect is functionally relevant if observed at the physiological pH range for cellular growth. The growth of *G. metallireducens* cells occurs in the pH range of 6.0–8.5, with optimum growth at pH 7 [45,46]. Therefore, to further rationalize the effect of the protonation/deprotonation of the redox-Bohr center in the functional mechanism of the cytochrome PpcA, the fractional contributions of the 16 microstates were

Biochemical Journal (2018) **475** 2861–2875
https://doi.org/10.1042/BCJ20180457

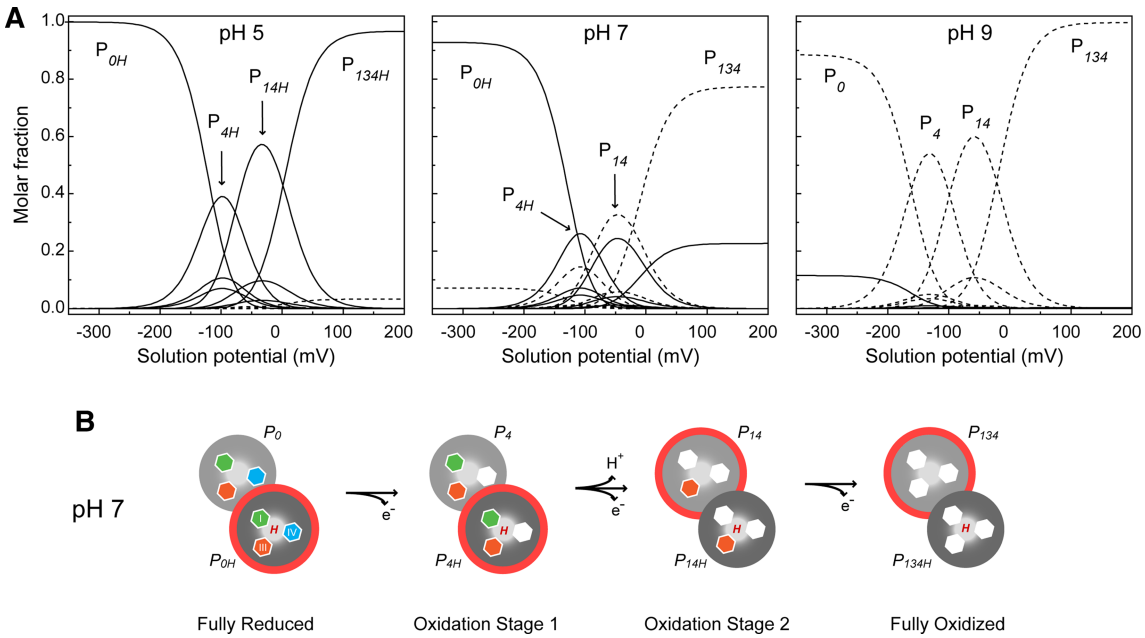

Figure 7. Electron/proton transfer pathways of PpcA from *G. metallireducens*.

(**A**) Redox-dependence of the molar fractions of the 16 microstates of the cytochrome, at different pH values. The curves were calculated as a function of the solution reduction potential (relative to NHE) using the parameters listed in Table 2. Solid and dashed lines indicate the protonated and deprotonated microstates, respectively (see Figure 2). For clarity, only the dominant microstates are labeled. (**B**) Preferential electron/proton-coupled transfer pathway of PpcA from *G. metallireducens*, at physiological pH. The figure is represented with the same features of Figure 2, although in a simpler extend, for clarity. The dominant microstates are highlighted by red circles.

determined at pH 5, 7 and 9 (Figure 7A). The analysis of this figure shows that the relevant microstates are quite distinct at different pH values. At values outside the physiological pH range, the dominant microstates are all protonated (pH 5) or deprotonated (pH 9). However, at pH 7, stage 0 is dominated by the protonated form P_{0H} and stage 1 is dominated by the oxidation of heme IV (P_{4H}), while keeping the redox-Bohr center protonated. Stage 2 is then dominated by the oxidation of heme I and deprotonation of the acid–base center (P_{14}), which remains deprotonated in stage 3 (P_{134}). Therefore, at pH 7, the following route is defined for the electrons: $P_{0H} \rightarrow P_{4H} \rightarrow P_{14} \rightarrow P_{134}$ (Figure 7B). This clearly indicates that at physiological pH, a concerted e^-/H^+ transfer occurs between oxidation stages 1 and 2.

Conclusions

In this work, we used NMR and visible spectroscopic techniques to probe the functional properties of the triheme cytochrome PpcA from *G. metallireducens*. To achieve this, the assignment of the heme methyl NMR signals was carried out for the fully reduced and oxidized states. These assignments constituted the starting points for the thermodynamic studies, performed by probing the heme methyl chemical shift variation during the protein oxidation at different pH values. These data, together with data obtained from visible redox titrations, were fitted with the thermodynamic model that allowed the determination of the heme reduction potentials, the heme interactions and the properties of the redox-Bohr center. The data obtained showed that the heme reduction potentials of the cytochrome PpcA are strongly modulated by heme–heme interactions and by interactions with the redox-Bohr center located in the vicinity of heme IV.

The order of oxidation of the hemes is pH-independent. However, the cytochrome is designed to perform e^-/H^+ transfer only within the cellular optimal pH range for growth, reinforcing the physiological significance of the redox-Bohr effect observed. Compared with other triheme cytochromes, the heme reduction potentials of PpcA from *G. metallireducens* are considerable less negative. Previous studies on *G. sulfurreducens* biofilms have shown that the electrochemical responses are mainly driven by the highly abundant periplasmic

cytochromes [47–49]. Overall, the data obtained for PpcA *G. metallireducens* suggest that the bacterium is optimized to function at less negative redox potential windows and the higher reduction potential values of the cytochrome also suggest that the electron transfer from cytoplasmic electron donors toward periplasmic cytochromes is accomplished with a higher driving force to confer extracellular electron transfer directionality.

Abbreviations

EXSY, EXchange SpectroscopY; NHE, Normal Hydrogen Electrode.

Author Contribution

T.M.F. and L.M. prepared the samples and acquired the NMR experiments. All the authors participated in the data analysis and treatment. T.M.F. and L.M. prepared all the figures. C.A.S. and T.M.F. wrote the manuscript. L. M. critically read and discussed the manuscript.

Funding

This work was supported by Fundação para a Ciência e Tecnologia (FCT) through the following grants: SFRH/BPD/114848/2016 (to L.M.) and PTDC/BBB-BQB/3554/2014 (to C.A.S.). This work was also supported by Unidade de Ciências Biomoleculares Aplicadas-UCIBIO, which is financed by national funds from FCT/MEC [UID/Multi/04378/2013] and co-financed by the ERDF under PT2020 Partnership Agreement [POCI-01-0145-FEDER-007728]. The NMR spectrometers are part of the National NMR Network (PTNMR) and are supported by Infrastructure Project N°022161 (co-financed by FEDER through COMPETE 2020, POCI, and PORL and FCT through PIDDAC).

Acknowledgements

Dr Raj P. Pokkuluri is thanked for helpful discussions and for critically reading the manuscript. Prof. David L. Turner is thanked for the thermodynamic model software.

Competing Interests

The Authors declare that there are no competing interests associated with the manuscript.

References

1 Lovley, D.R., Ueki, T., Zhang, T., Malvankar, N.S., Shrestha, P.M., Flanagan, K.A. et al. (2011) *Geobacter*: the microbe electric's physiology, ecology, and practical applications. *Adv. Microb. Physiol.* **59**, 1–100 https://doi.org/10.1016/B978-0-12-387661-4.00004-5

2 Gregory, K.B. and Lovley, D.R. (2005) Remediation and recovery of uranium from contaminated subsurface environments with electrodes. *Environ. Sci. Technol.* **39**, 8943–8947 https://doi.org/10.1021/es050457e

3 Lovley, D.R., Baedecker, M.J., Lonergan, D.J., Cozzarelli, I.M., Phillips, E.J.P. and Siegel, D.I. (1989) Oxidation of aromatic contaminants coupled to microbial iron reduction. *Nature* **339**, 297–300 https://doi.org/10.1038/339297a0

4 N'Guessan, A.L., Vrionis, H.A., Resch, C.T., Long, P.E. and Lovley, D.R. (2008) Sustained removal of uranium from contaminated groundwater following stimulation of dissimilatory metal reduction. *Environ. Sci. Technol.* **42**, 2999–3004 https://doi.org/10.1021/es071960p

5 Williams, K.H., Long, P.E., Davis, J.A., Wilkins, M.J., N'Guessan, A.L., Steefel, C.I. et al. (2011) Acetate availability and its influence on sustainable bioremediation of uranium-contaminated groundwater. *Geomicrobiol. J.* **28**, 519–539 https://doi.org/10.1080/01490451.2010.520074

6 Zhang, T., Gannon, S.M., Nevin, K.P., Franks, A.E. and Lovley, D.R. (2010) Stimulating the anaerobic degradation of aromatic hydrocarbons in contaminated sediments by providing an electrode as the electron acceptor. *Environ. Microbiol.* **12**, 1011–1020 https://doi.org/10.1111/j.1462-2920.2009.02145.x

7 Coates, J.D., Woodward, J., Allen, J., Philp, P. and Lovley, D.R. (1997) Anaerobic degradation of polycyclic aromatic hydrocarbons and alkanes in petroleum-contaminated marine harbor sediments. *Appl. Environ. Microbiol.* **63**, 3589–3593 https://www.ncbi.nlm.nih.gov/pubmed/9341091

8 Nevin, K.P., Richter, H., Covalla, S.F., Johnson, J.P., Woodard, T.L., Orloff, A.L. et al. (2008) Power output and columbic efficiencies from biofilms of *Geobacter sulfurreducens* comparable to mixed community microbial fuel cells. *Environ. Microbiol.* **10**, 2505–2514 https://doi.org/10.1111/j.1462-2920.2008.01675.x

9 Lloyd, J.R. and Lovley, D.R. (2001) Microbial detoxification of metals and radionuclides. *Curr. Opin. Biotechnol.* **12**, 248–253 https://doi.org/10.1016/S0958-1669(00)00207-X

10 Lovley, D.R. (1993) Dissimilatory metal reduction. *Annu. Rev. Microbiol.* **47**, 263–290 https://doi.org/10.1146/annurev.mi.47.100193.001403

11 Coppi, M.V., Leang, C., Sandler, S.J. and Lovley, D.R. (2001) Development of a genetic system for *Geobacter sulfurreducens*. *Appl. Environ. Microbiol.* **67**, 3180–3187 https://doi.org/10.1128/AEM.67.7.3180-3187.2001

12 Ding, Y.-H.R., Hixson, K.K., Aklujkar, M.A., Lipton, M.S., Smith, R.D., Lovley, D.R. et al. (2008) Proteome of *Geobacter sulfurreducens* grown with Fe(III) oxide or Fe(III) citrate as the electron acceptor. *Biochim. Biophys. Acta, Proteins Proteomics* **1784**, 1935–1941 https://doi.org/10.1016/j.bbapap.2008.06.011

13 Ding, Y.-H., Hixson, K.K., Giometti, C.S., Stanley, A., Esteve-Núñez, A., Khare, T. et al. (2006) The proteome of dissimilatory metal-reducing microorganism *Geobacter sulfurreducens* under various growth conditions. *Biochim. Biophys. Acta, Proteins Proteomics* **1764**, 1198–1206 https://doi.org/10.1016/j.bbapap.2006.04.017

Biochemical Journal (2018) **475** 2861–2875
https://doi.org/10.1042/BCJ20180457

14 Kim, B.-C., Leang, C., Ding, Y.-H.R., Glaven, R.H., Coppi, M.V. and Lovley, D.R. (2005) Omcf, a putative *c*-type monoheme outer membrane cytochrome required for the expression of other outer membrane cytochromes in *Geobacter sulfurreducens*. *J. Bacteriol.* **187**, 4505–4513 https://doi.org/10.1128/JB.187.13.4505-4513.2005

15 Lloyd, J.R., Leang, C., Hodges Myerson, A.L.H., Coppi, M.V., Cuifo, S., Methe, B. et al. (2003) Biochemical and genetic characterization of PpcA, a periplasmic *c*-type cytochrome in *Geobacter sulfurreducens*. *Biochem. J.* **369**, 153–161 https://doi.org/10.1042/bj20020597

16 Park, I. and Kim, B.-C. (2011) Homologous overexpression of *omcZ*, a gene for an outer surface *c*-type cytochrome of *Geobacter sulfurreducens* by single-step gene replacement. *Biotechnol. Lett.* **33**, 2043–2048 https://doi.org/10.1007/s10529-011-0668-7

17 Rollefson, J.B., Levar, C.E. and Bond, D.R. (2009) Identification of genes involved in biofilm formation and respiration via mini-*Himar* transposon mutagenesis of *Geobacter sulfurreducens*. *J. Bacteriol.* **191**, 4207–4217 https://doi.org/10.1128/JB.00057-09

18 Ueki, T. and Lovley, D.R. (2010) Genome-wide gene regulation of biosynthesis and energy generation by a novel transcriptional repressor in *Geobacter* species. *Nucleic Acids Res.* **38**, 810–821 https://doi.org/10.1093/nar/gkp1085

19 Lovley, D.R., Giovannoni, S.J., White, D.C., Champine, J.E., Phillips, E.J.P., Gorby, Y.A. et al. (1993) *Geobacter metallireducens* gen. nov. sp. nov., a microorganism capable of coupling the complete oxidation of organic compounds to the reduction of iron and other metals. *Arch. Microbiol.* **159**, 336–344 https://doi.org/10.1007/BF00290916

20 Lovley, D.R., Stolz, J.F., Nord, Jr, G.L. and Phillips, E.J.P. (1987) Anaerobic production of magnetite by a dissimilatory iron-reducing microorganism. *Nature* **330**, 252–254 https://doi.org/10.1038/330252a0

21 Lovley, D.R. and Phillips, E.J. (1988) Novel mode of microbial energy metabolism: organic carbon oxidation coupled to dissimilatory reduction of iron or manganese. *Appl. Environ. Microbiol.* **54**, 1472–1480 PMID:16347658

22 Tobler, N.B., Hofstetter, T.B. and Schwarzenbach, R.P. (2008) Carbon and hydrogen isotope fractionation during anaerobic toluene oxidation by *Geobacter metallireducens* with different Fe(III) phases as terminal electron acceptors. *Environ. Sci. Technol.* **42**, 7786–7792 https://doi.org/10.1021/es800046z

23 Aklujkar, M., Krushkal, J., DiBartolo, G., Lapidus, A., Land, M.L. and Lovley, D.R. (2009) The genome sequence of *Geobacter metallireducens*: features of metabolism, physiology and regulation common and dissimilar to *Geobacter sulfurreducens*. *BMC Microbiol.* **9**, 109 https://doi.org/10.1186/1471-2180-9-109

24 Wiatrowski, H.A., Ward, P.M. and Barkay, T. (2006) Novel reduction of mercury(II) by mercury-sensitive dissimilatory metal reducing bacteria. *Environ. Sci. Technol.* **40**, 6690–6696 https://doi.org/10.1021/es061046g

25 Kashima, H. and Regan, J.M. (2015) Facultative nitrate reduction by electrode-respiring *Geobacter metallireducens* biofilms as a competitive reaction to electrode reduction in a bioelectrochemical system. *Environ. Sci. Technol.* **49**, 3195–3202 https://doi.org/10.1021/es504882f

26 Senko, J.M. and Stolz, J.F. (2001) Evidence for iron-dependent nitrate respiration in the dissimilatory iron-reducing bacterium *Geobacter metallireducens*. *Appl. Environ. Microbiol.* **67**, 3750–3752 https://doi.org/10.1128/AEM.67.8.3750-3752.2001

27 Tremblay, P.-L., Aklujkar, M., Leang, C., Nevin, K.P. and Lovley, D. (2012) A genetic system for *Geobacter metallireducens*: role of the flagellin and pilin in the reduction of Fe(III) oxide. *Environ. Microbiol. Rep.* **4**, 82–88 https://doi.org/10.1111/j.1758-2229.2011.00305.x

28 Aklujkar, M., Coppi, M.V., Leang, C., Kim, B.C., Chavan, M.A., Perpetua, L.A. et al. (2013) Proteins involved in electron transfer to Fe(III) and Mn(IV) oxides by *Geobacter sulfurreducens* and *Geobacter uraniireducens*. *Microbiology* **159**(Pt_3), 515–535 https://doi.org/10.1099/mic.0.064089-0

29 Inoue, K., Leang, C., Franks, A.E., Woodard, T.L., Nevin, K.P. and Lovley, D.R. (2011) Specific localization of the *c*-type cytochrome OmcZ at the anode surface in current-producing biofilms of *Geobacter sulfurreducens*. *Environ. Microbiol. Rep.* **3**, 211–217 https://doi.org/10.1111/j.1758-2229.2010.00210.x

30 Kim, B.-C. and Lovley, D.R. (2008) Investigation of direct vs. indirect involvement of the *c*-type cytochrome MacA in Fe(III) reduction by *Geobacter sulfurreducens*. *FEMS Microbiol. Lett.* **286**, 39–44 https://doi.org/10.1111/j.1574-6968.2008.01252.x

31 Levar, C.E., Chan, C.H., Mehta-Kolte, M.G. and Bond, D.R. (2014) An inner membrane cytochrome required only for reduction of high redox potential extracellular electron acceptors. *mBio* **5**, e02034 https://doi.org/10.1128/mBio.02034-14

32 Liu, Y., Fredrickson, J.K., Zachara, J.M. and Shi, L. (2015) Direct involvement of *ombB*, *omaB*, and *omcB* genes in extracellular reduction of Fe(III) by *Geobacter sulfurreducens* PCA. *Front. Microbiol.* **6**, 1075 https://doi.org/10.3389/fmicb.2015.01075

33 Mehta, T., Coppi, M.V., Childers, S.E. and Lovley, D.R. (2005) Outer membrane *c*-type cytochromes required for Fe(III) and Mn(IV) oxide reduction in *Geobacter sulfurreducens*. *Appl. Environ. Microbiol.* **71**, 8634–8641 https://doi.org/10.1128/AEM.71.12.8634-8641.2005

34 Nevin, K.P., Kim, B.-C., Glaven, R.H., Johnson, J.P., Woodard, T.L., Methé, B.A. et al. (2009) Anode biofilm transcriptomics reveals outer surface components essential for high density current production in *Geobacter sulfurreducens* fuel cells. *PLoS ONE* **4**, e5628 https://doi.org/10.1371/journal.pone.0005628

35 Zacharoff, L., Chan, C.H. and Bond, D.R. (2016) Reduction of low potential electron acceptors requires the CbcL inner membrane cytochrome of *Geobacter sulfurreducens*. *Bioelectrochemistry* **107**, 7–13 https://doi.org/10.1016/j.bioelechem.2015.08.003

36 Afkar, E. and Fukumori, Y. (1999) Purification and characterization of triheme cytochrome c_7 from the metal-reducing bacterium, *Geobacter metallireducens*. *FEMS Microbiol. Lett.* **175**, 205–210 https://doi.org/10.1111/j.1574-6968.1999.tb13621.x

37 Smith, J.A., Lovley, D.R. and Tremblay, P.-L. (2013) Outer cell surface components essential for Fe(III) oxide reduction by *Geobacter metallireducens*. *Appl. Environ. Microbiol.* **79**, 901–907 https://doi.org/10.1128/AEM.02954-12

38 Butler, J.E., Young, N.D. and Lovley, D.R. (2010) Evolution of electron transfer out of the cell: comparative genomics of six *Geobacter* genomes. *BMC Genomics* **11**, 40 https://doi.org/10.1186/1471-2164-11-40

39 Portela, P.C., Fernandes, T.M., Dantas, J.M., Ferreira, M.R. and Salgueiro, C.A. (2018) Biochemical and functional insights on the triheme cytochrome PpcA from *Geobacter metallireducens*. *Arch. Biochem. Biophys.* **644**, 8–16 https://doi.org/10.1016/j.abb.2018.02.017

40 Turner, D.L., Salgueiro, C.A., Catarino, T., Legall, J. and Xavier, A.V. (1996) NMR studies of cooperativity in the tetrahaem cytochrome c_3 from *Desulfovibrio vulgaris*. *Eur. J. Biochem.* **241**, 723–731 https://doi.org/10.1111/j.1432-1033.1996.00723.x

41 Morgado, L., Dantas, J.M., Bruix, M., Londer, Y.Y. and Salgueiro, C.A. (2012) Fine tuning of redox networks on multiheme cytochromes from *Geobacter sulfurreducens* drives physiological electron/proton energy transduction. *Bioinorg. Chem. Appl.* **2012**, 298739 https://doi.org/10.1155/2012/298739

42 Morgado, L., Saraiva, I.H., Louro, R.O. and Salgueiro, C.A. (2010) Orientation of the axial ligands and magnetic properties of the hemes in the triheme ferricytochrome PpcA from *G. sulfurreducens* determined by paramagnetic NMR. *FEBS Lett.* **584**, 3442–3445 https://doi.org/10.1016/j.febslet.2010.06.043

43 Salgueiro, C.A., Turner, D.L. and Xavier, A.V. (1997) Use of paramagnetic NMR probes for structural analysis in cytochrome c_3 from *Desulfovibrio vulgaris*. *Eur. J. Biochem.* **244**, 721–734 https://doi.org/10.1111/j.1432-1033.1997.00721.x
44 Turner, D.L., Salgueiro, C.A., Schenkels, P., LeGall, J. and Xavier, A.V. (1995) Carbon-13 NMR studies of the influence of axial ligand orientation on haem electronic structure. *Biochim. Biophys. Acta, Protein Struct. Mol. Enzymol.* **1246**, 24–28 https://doi.org/10.1016/0167-4838(94)00175-G
45 Sun, D., Wang, A., Cheng, S., Yates, M. and Logan, B.E. (2014) *Geobacter anodireducens* sp. nov., an exoelectrogenic microbe in bioelectrochemical systems. *Int. J. Syst. Evol. Microbiol.* **64**(Pt 10), 3485–3491 https://doi.org/10.1099/ijs.0.061598-0
46 Sun, J., Sayyar, B., Butler, J.E., Pharkya, P., Fahland, T.R., Famili, I. et al. (2009) Genome-scale constraint-based modeling of *Geobacter metallireducens*. *BMC Syst. Biol.* **3**, 15 https://doi.org/10.1186/1752-0509-3-15
47 Liu, Y., Kim, H., Franklin, R.R. and Bond, D.R. (2011) Linking spectral and electrochemical analysis to monitor *c*-type cytochrome redox status in living *Geobacter sulfurreducens* biofilms. *ChemPhysChem* **12**, 2235–2241 https://doi.org/10.1002/cphc.201100246
48 Marsili, E., Rollefson, J.B., Baron, D.B., Hozalski, R.M. and Bond, D.R. (2008) Microbial biofilm voltammetry: direct electrochemical characterization of catalytic electrode-attached biofilms. *Appl. Environ. Microbiol.* **74**, 7329–7337 https://doi.org/10.1128/AEM.00177-08
49 Srikanth, S., Marsili, E., Flickinger, M.C. and Bond, D.R. (2008) Electrochemical characterization of *Geobacter sulfurreducens* cells immobilized on graphite paper electrodes. *Biotechnol. Bioeng.* **99**, 1065–1073 https://doi.org/10.1002/bit.21671
50 Morgado, L., Bruix, M., Pessanha, M., Londer, Y.Y. and Salgueiro, C.A. (2010) Thermodynamic characterization of a triheme cytochrome family from *Geobacter sulfurreducens* reveals mechanistic and functional diversity. *Biophys. J.* **99**, 293–301 https://doi.org/10.1016/j.bpj.2010.04.017
51 Correia, I.J., Paquete, C.M., Louro, R.O., Catarino, T., Turner, D.L. and Xavier, A.V. (2002) Thermodynamic and kinetic characterization of trihaem cytochrome c_3 from *Desulfuromonas acetoxidans*. *Eur. J. Biochem.* **269**, 5722–5730 https://doi.org/10.1046/j.1432-1033.2002.03286.x
52 Moss, G.P. (1988) Nomenclature of tetrapyrroles. Recommendations. *Eur. J. Biochem.* **178**, 277–328 https://doi.org/10.1111/j.1432-1033.1988.tb14453.x
53 Morgado, L., Bruix, M., Pokkuluri, P.R., Salgueiro, C.A. and Turner, D.L. (2017) Redox- and pH-linked conformational changes in triheme cytochrome PpcA from *Geobacter sulfurreducens*. *Biochem. J.* **474**, 231–246 https://doi.org/10.1042/BCJ20160932
54 Turner, D.L., Costa, H.S., Coutinho, I.B., Legall, J. and Xavier, A.V. (1997) Assignment of the ligand geometry and redox potentials of the trihaem ferricytochrome c_3 from *Desulfuromonas acetoxidans*. *Eur. J. Biochem.* **243**, 474–481 https://doi.org/10.1111/j.1432-1033.1997.0474a.x